ELSEVIER

Chemical Engineering and Processing 42 (2003) 211–221

Chemical Engineering and Processing

www.elsevier.com/locate/cep

Bifurcation analysis for TAME synthesis in a reactive distillation column: comparison of pseudo-homogeneous and heterogeneous reaction kinetics models

R. Baur [a], R. Taylor [b], R. Krishna [a,*]

[a] *Department of Chemical Engineering, University of Amsterdam, Nieuwe Achtergracht 166, 1018 WV Amsterdam, The Netherlands*
[b] *Department of Chemical Engineering, Clarkson University, Potsdam, NY 13699-5705, USA*

Received 24 July 2001; received in revised form 18 January 2002; accepted 15 March 2002

Abstract

This paper presents a bifurcation analysis for synthesis of tertiary amyl ether (TAME) in a reactive distillation (RD) column. Two different methods for describing the reaction kinetics are explored and compared: (A) *pseudo-homogeneous models:* here the intra-particle diffusion and reaction is simplified by the use of catalyst effectiveness factors and pseudo-homogeneous rate expressions, and (B) *heterogeneous models:* here detailed account is taken of intra-particle diffusion, using the dusty fluid model, and reaction within the catalyst particles. Both pseudo-homogeneous and heterogeneous reaction models show the possibility of multiple steady states. The bifurcation characteristics obtained with the two models are similar in nature and the essential features of the heterogeneous model can be captured with the pseudo-homogenous model by defining an appropriate value for the catalyst effectiveness factor, the value of which depends on the particular branch of the bifurcation diagram. The pseudo-homogeneous model was then applied to study the dynamics of a TAME synthesis RD column. Starting at the low conversion steady state, a feed composition perturbation is shown to lead to a transition to the high conversion steady state, in qualitative agreement with the experiments of Mohl et al. (Chem. Eng. Sci. 54 (1999) 1029). The quantitative differences in the dynamic responses are to be ascribed to imprecise knowledge of hydrodynamics, especially as concerns the static liquid hold-up in the RD column.

Keywords: Reactive distillation; Nonequilibrium stage model; Multiple steady states; Dusty fluid model; Pseudo-homogenous kinetics; Maxwell–Stefan equations; Tertiary-amyl ether synthesis; Non-linear dynamics

1. Introduction

Reactive distillation (RD) is an old idea that has received renewed attention in recent years; witness the recent reviews of Doherty and Malone [1,2] and Taylor and Krishna [3]. In the area of RD column design, research has mainly been focussed on aspects such as conceptual design with the aid of residue curve maps [1,2,4], steady-state multiplicity and bifurcations [5–9], development of equilibrium (EQ) stage and rigorous nonequilibrium (NEQ) steady state and dynamic models [10–33].

Fig. 1 shows schematically the various transport resistances encountered on any given stage of an RD column. With respect to the treatment of reaction kinetics, the published models fall into two classes:

A) *Pseudo-homogeneous models:* here the intra-particle diffusion and reaction is simplified by the use of catalyst effectiveness factors and pseudo-homogeneous rate expressions
B) *Heterogeneous models:* here detailed account is taken of intra-particle diffusion and reaction within the catalyst particles

With respect to the treatment of interphase and intraphase mass transfer, several approaches have been adopted in the published literature:

* Corresponding author. Fax: +31-20-5255604
E-mail address: krishna@science.uva.nl (R. Krishna).

0255-2701/03/$ - see front matter
PII: S0255-2701(02)00090-9

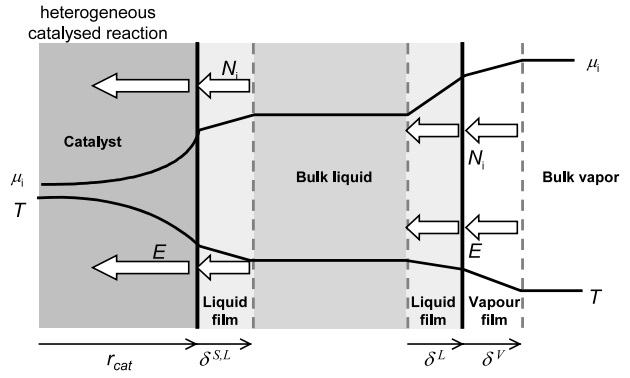

Fig. 1. Schematic depiction of a heterogeneous model; adapted from Taylor and Krishna [3].

1) *EQ stage models:* Here the vapour and liquid phases on any given stage are assumed to be in thermodynamic equilibrium. Such EQ models invariably adopt the pseudo-homogenous description of reaction kinetics.
2) *EQ stage models with overall stage efficiencies or HETPs:* In such models the vapour–liquid mass transfer process is accounted for in an overall manner by defining overall stage efficiencies or HETPs. No distinctions are made in the differences in the constituent mass transfer rates.
3) *NEQ stage models:* In such models the Maxwell–Stefan diffusion equations are almost invariably used to describe the interphase mass transfer process. Both pseudo-homogeneous and heterogeneous description of reaction kinetics have been incorporated in the NEQ stage model implementations.

The first major objective of our paper is to compare the predictions of rigorous pseudo-homogenous and heterogeneous NEQ stage models as regards the steady-state bifurcation characteristics. The second objective is to consider the dynamics of RD columns and to examine the extent to which pseudo-homogeneous models are adequate for use in practice. For illustration purposes we choose the specific example of the synthesis of tertiary-amyl ether (TAME), for which detailed experimental results, including column dynamics, have been published by Mohl et al. [33]. All the simulations to be presented below pertain to the RD column configuration of Mohl et al. [33].

2. Comparison of pseudo-homogeneous and heterogeneous models under steady-state

Fig. 1 schematically depicts the heterogeneous model as developed by Higler et al. [19]. Resistances to interfacial mass and energy transfer are assumed to be located in thin 'films' adjacent to the vapour–liquid interface and to the catalyst–liquid interface. The liquid phase diffusion film thickness δ^{L} is of the order of 10 μm and the vapour phase diffusion film thickness δ^{V} is of the order of 100 μm. The storage capacity for mass and energy in these films is negligibly small compared to that in the bulk fluid phases and so the interfacial transfer rates can be calculated from quasi-stationary interfacial transfer relations. The molar transfer rates in the films are related to the chemical potential gradients by the Maxwell–Stefan equations [3,34]. In case of a homogenous RD the coupling of diffusion and chemical reaction within the liquid film is particularly important for fast chemical reactions (Hatta number exceeding unity). For solid catalysed chemical reactions our approach is to use the dusty fluid model in order to account for intra-catalyst diffusion and reaction in the catalyst [19,28–31]. In such cases there will be no coupling of chemical reaction and diffusion within the liquid film. The dusty fluid model is a modification of the dusty gas model with the aim of describing liquid phase diffusion in porous media [34]. The porous material is described as a supplementary 'dust' species consisting of large motionless molecules held motionless in space. The fluxes within the catalyst particle are given by (Eq. (38) of Higler et al. [19])

$$-\frac{x_i}{RT}\nabla_{T,p}\mu_i - \frac{x_i}{RT}\left(\overline{V}_i + \frac{B_0}{\eta \mathcal{D}^e_{iM}}\right)\nabla p = \sum_{\substack{j=1\\ j\neq i}}^{n} \frac{x_j\mathbf{N}_i - x_i\mathbf{N}_j}{c_t \mathcal{D}^e_{ij}} + \frac{\mathbf{N}_i}{c_t \mathcal{D}^e_{iM}} \qquad (1)$$

$$i = 1, 2, \ldots n$$

There are, in general, two types of diffusivities to reckon with: (1) $\mathcal{D}^e_{ij}$ representing the liquid phase diffusivity of i–j pair within the catalyst particle, and (2) $\mathcal{D}^e_{iM}$ reflecting the interaction of species i with the catalyst walls; this is the Knudsen diffusivity. The $\mathcal{D}^e_{ij}$ can be estimated from knowledge of the bulk liquid phase diffusivity $\mathcal{D}_{ij}$:

$$\mathcal{D}^e_{ij} = \frac{\varepsilon}{\tau}\mathcal{D}_{ij} \qquad (2)$$

The estimation of the Knudsen diffusivity $\mathcal{D}^e_{iM}$ is much more difficult. Sundmacher et al. [28–31] ignore the Knudsen diffusivities in their formulations assuming $\mathcal{D}^e_{iM} \to \infty$. In the simulation results to be presented below we also use this simplification to start with. To study the influence of Knudsen contribution we have also tested two other scenarios: (1) $\mathcal{D}^e_{iM}$ is identical for all species and equal to the arithmetic average of the $\mathcal{D}^e_{ij}$, (2) $\mathcal{D}^e_{iM}$ is five times the value obtained in scenario (1).

The permeability B_0 in Eq. (1) can be estimated from knowledge of the pore diameter, d_{p};

$$B_0 = \frac{d_p^2}{32} \quad (3)$$

Solving Eq. (1) requires additional information about the catalyst, such as catalyst thickness, geometry, porosity and tortuosity.

The commonly used pseudo-homogenous model is a computationally less expensive alternative to the rigorous description of the dusty fluid model. Heterogeneous chemical reactions taking place inside catalyst particles are taken account of by use of 'effective' reaction rate constants.

Both models, pseudo-homogenous and heterogeneous model, require thermodynamic properties, not only for calculation of phase EQ but also for calculation of driving forces for mass transfer and, in RD, for taking into account the effect of non-ideal component behaviour in the calculation of reaction rates and chemical EQ constants. In addition, physical properties such as surface tension, diffusion coefficients, viscosities, etc. for calculation of mass (and heat) transfer coefficients and interfacial areas are required. For the most part the property models we use are those recommended by Reid et al. [35] and by Danner and Daubert [36]. The details of the models used for estimation of diffusivities are discussed in standard texts [35,37].

For dynamic simulations, using the pseudo-homogenous NEQ model, to be presented later, hardware design information must be specified so that mass transfer coefficients, interfacial areas, liquid hold-ups and pressure drops can be calculated. A listing of the correlations for tray and packed columns implemented in the program are given in Kooijman and Taylor [38], which also contains details of all thermodynamics, hydrodynamics and mass transfer models for tray and packed columns which have already been implemented into our RD software. The code for these models represents a large fraction of the overall program size.

The resulting set of differential–algebraic (DAE) equations is solved using BESIRK [39]. BESIRK is a semi-implicit Runge-Kutta method originally developed by Michelsen [40] and extended with an extrapolation scheme [41], improving the efficiency in solving the DAE problem. The evaluation of the sparse Jacobian is primarily based on analytical expressions, except for the computation of entries for correlations like enthalpies, mass and heat transfer coefficients, hold-ups and pressure drops.

Our program also supports steady state computations using Newton's method, as outlined in Taylor et al. [42]. In addition, the program is equipped with a continuation method for analysis of multiple-steady state behaviour. For more details about this continuation method the reader is referred to Wayburn and Seader [43] and Kubicek [44].

3. Steady-state multiplicity for TAME synthesis

We first examine the steady-state multiplicity characteristics of the TAME process using both the pseudo-homogeneous and heterogeneous descriptions of the catalytic reactions. TAME is formed by reversible, acid-catalysed, exothermic reaction of iso-amylenes, consisting of the isomers 2-methyl-1-butene (2M1B) and 2-methyl-2-butene (2M2B), with methanol

$$\text{methanol} + \text{2M1B} \leftrightarrow \text{TAME} \quad (4a)$$

$$\text{methanol} + \text{2M2B} \leftrightarrow \text{TAME} \quad (4b)$$

The reaction kinetics has been studied by two different groups in Clausthal [4,31–33,45,46] and in Helsinki [47–49]. In our simulations we use the forward reaction rate constants as presented by the Clausthal group; the reaction kinetics is described by a Langmuir–Hinshelwood rate expression in terms of the liquid phase activities [4,31–33,45,46]. The reaction EQ constant has been calculated according to Rihko and Krause [47]. We did not incorporate the isomerization reaction of the C5-olefins in our model. The catalyst activity has been specified by 900 eq$[H^+]/m^3$; the overall catalyst volume depends on the type of packing and voidage in the column and the complete catalyst volume to be 1.2 l.

Fig. 2(a) schematically depicts the column configuration of the TAME process presented in Mohl et al. [33]. The column has an inner diameter of 76 mm. The top section of the column is packed with catalytic and the bottom section with inert (glass) Raschig rings. Both sections are 0.5 m high. The feed is located in the middle of the column between the reactive and inert packing. As specified by Mohl et al. [33] in their experiments the feed rate was chosen to be 0.96 kg/h. The column operates at a pressure of 0.25 MPa. The Wilson equation was used for calculating the liquid activity coefficients. Furthermore, a total condenser and total reboiler are employed. The reflux ratio was specified at 15, whereas the reboiler heat duty was used as a homotopy parameter. Each section has been divided in 20 slices. Simulations with the pseudo-homogenous model show that the overall performance correspond to an EQ stage model with 10 stages and an efficiency of 0.7 proposed and experimentally validated by Mohl et al. [33]. The column configuration was subsequently maintained the same for both pseudo-homogenous and heterogeneous model.

In the experiments, Mohl et al. [33] experimentally observed steady-state multiplicity for a reboiler load of 340 W; the two steady states differ in their temperature profile and TAME purity in bottoms flow rate. The high-conversion steady state (HSS) denotes the steady state with higher temperatures and higher TAME purity. By contrast the low conversion steady state (LSS) has lower temperatures and lower TAME purity. The experimentally measured temperature profiles for

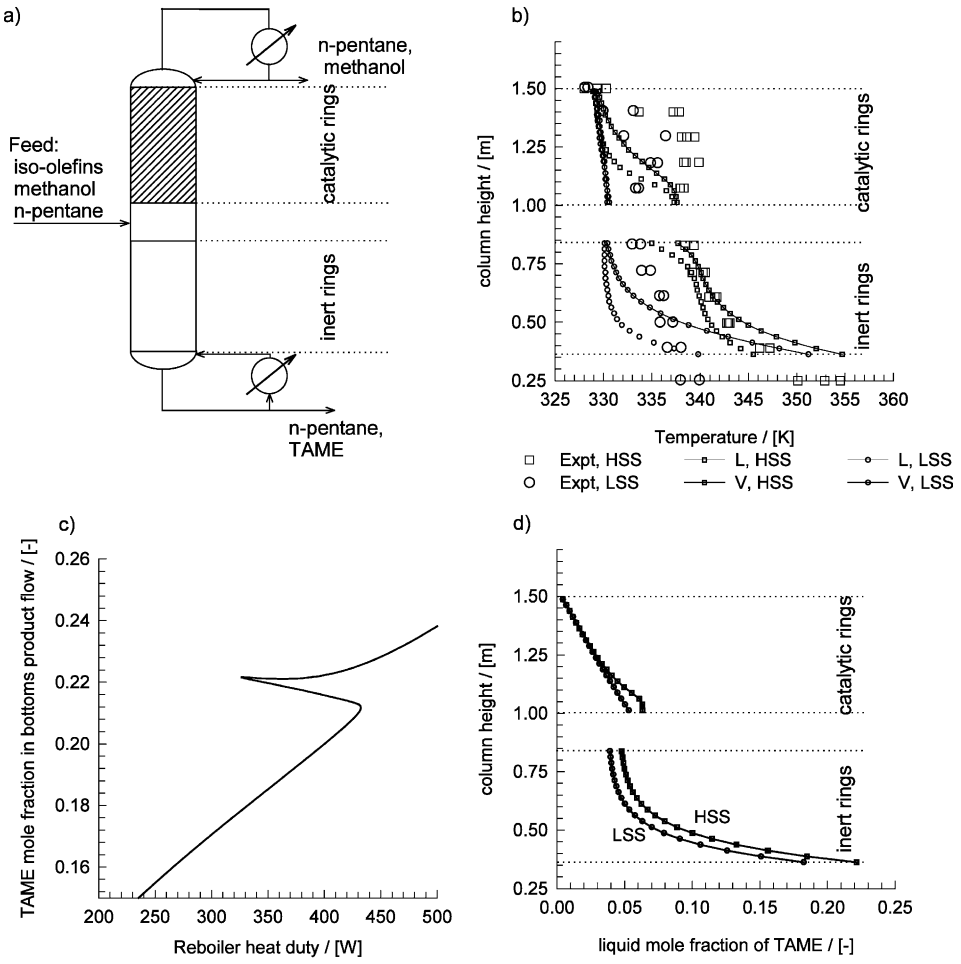

Fig. 2. (a) Schematic depiction of the column configuration used by Mohl et al. [33]. (b) Temperature profiles of the HSS and LSS at a reboiler load of 340 W, (c) bifurcation diagram for the pseudo-homogenous model. (d) Steady-state profiles of the TAME liquid composition.

the two steady states, HSS and LSS, are shown respectively by the larger open square and circles symbols in Fig. 2(b). As the temperatures have been measured by means of a thermocouple placed inside the column, it is not possible to specify whether the temperatures refer to the vapour or liquid phases. It is likely that the thermocouples record the higher of the two temperatures. We developed the bifurcation diagram for the RD column using the reboiler load as continuation parameter; the simulation results are shown in Fig. 2(c). It is clear that at a reboiler load of 340 W, we have steady-state multiplicity, in conformity with the experiments. With this reboiler load of 340 W, the RD column was simulated using a pseudo-homogeneous model and the corresponding temperature profiles are shown in Fig. 2(b). In our simulations there is a finite difference between the vapour and liquid temperatures. This difference is due to the fact that the heat transfer between the gas and liquid phases in the laboratory column is not high. We note that the vapour temperature is higher than the liquid temperature. The simulated vapour temperatures are closer to the experimentally determined values than the liquid temperatures. This is understandable in view of the fact that the thermocouples probably sense the higher of the two temperatures. We also note that the agreement in the temperature profiles between the experiments and simulations is not very good. The simulated values of the liquid phase mole fraction are shown in Fig. 2(d) for both HSS and LSS. The TAME mole fraction in the bottoms product is about 0.2214 for the HSS and 0.1824 for the LSS, respectively. These values agree with the trends in the experimental values reported by Mohl et al. [33].

For comparison purposes we also carried out simulations of the steady-state behaviour using heterogeneous dusty fluid model of Higler et al. [19] employing the same reaction kinetics as for the pseudo-homogeneous model simulations in Fig. 2. The catalyst parameters used are: packing voidage = 0.47; catalyst porosity = 0.39, tortuosity = 1.5, catalyst surface area = 567 m^2/m^3, mean pore diameter = 160 nm, catalyst thickness = 2 mm, thermal conductivity = 1.0×10^{-6} J/K/m/s. The parameter values are based on specifications given in

Mohl et al. [33], Rapmund et al. [32] and Sundmacher [28]. In order to solve the partial differential equations along the film and catalyst thickness numerically, we applied a finite difference scheme. Detailed description of the model and discretization scheme is given in Higler et al. [19]. For the discretization of the catalyst thickness we applied 50 grid points in the catalyst layer (of thickness 2 mm in the base case) per column slice. Finer grid spacing does not alter the results.

Fig. 3 shows the bifurcation diagram of the TAME purity in the bottoms flow rate when the reboiler load is varied for both models. In the base case calculations we took the dusty fluid parameters as specified above. Furthermore, we ignored the Knudsen terms in the dusty fluid formulation; the simulations therefore reduce to the formulation of Sundmacher and Hoffmann [28,29]. The pseudo-homogenous model and the dusty fluid model exhibit similar steady-state multiplicity characteristics. The additional intra-particle mass and heat transfer resistances cause the overall TAME production of the dusty fluid model to be lower, as can be expected. Furthermore, the dusty fluid model degenerates to the pseudo-homogenous model as intra-catalyst resistances vanish. In this case the pressure and composition gradients within the catalyst particle disappear and the reaction rate becomes constant within the catalyst. The intra-catalyst diffusion resistance can be influenced by changing (1) the interfacial area of catalyst per m^3 packing, (2) tortuosity, (3) catalyst thickness, and (4) the Knudsen diffusivity in the dusty fluid Model. In Fig. 3(a) we show the influence of varying the specific interfacial area of the catalyst. As the specific interfacial area is increased from 567 m^2/m^3 to 10 000 m^2/m^3 the bifurcation characteristics of the dusty fluid model coincides exactly with that of the pseudo-homogeneous model. This provides a good check of the dusty fluid model.

Fig. 3(b) shows the influence of varying the tortuosity from 1.5 (base case). Decreasing the tortuosity to 1 makes the dusty fluid model results approach that of the pseudo-homogenous model but the influence is far less than that of increasing catalyst specific area. Increasing the catalyst tortuosity has the opposite effect. The influence of varying catalyst thickness is shown in Fig. 3(c). We note that decreasing the catalyst thickness reduces the intra-catalyst resistance and the TAME production moves closer to the results of the pseudo-homogeneous model. Increasing the catalyst thickness

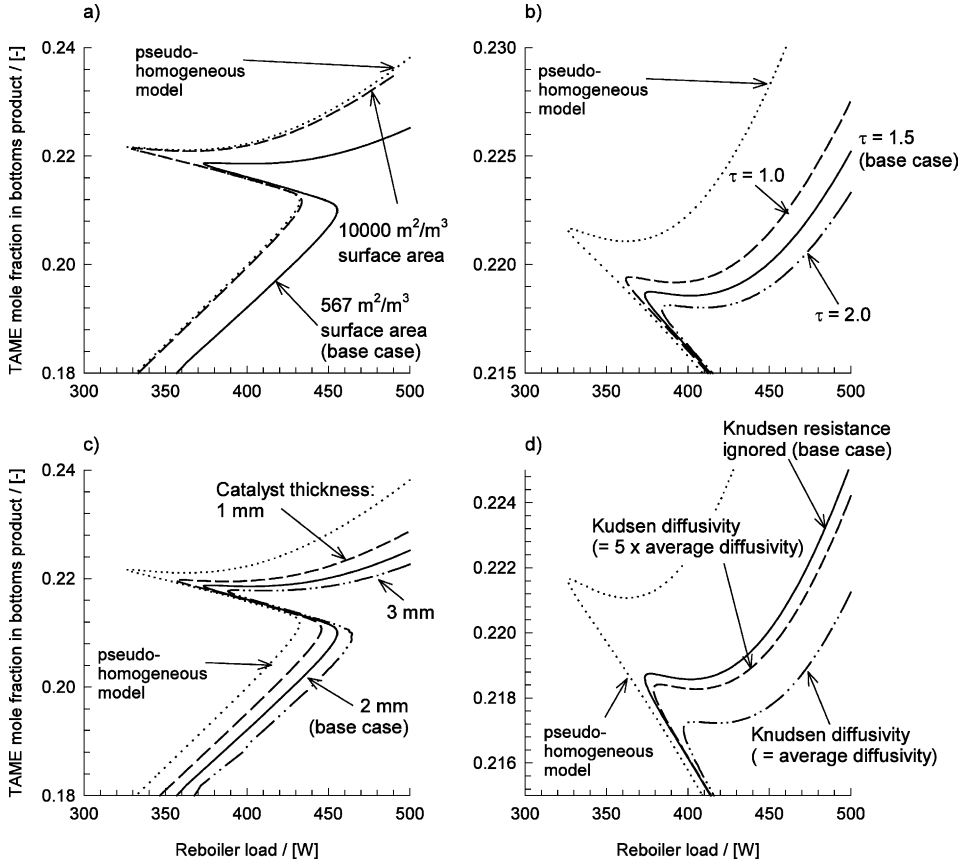

Fig. 3. Bifurcation diagrams of the dusty fluid model for parameter variation of (a) specific catalyst area, (b) tortuosity, (c) catalyst thickness and (d) Knudsen diffusivity. The base case corresponds to the dusty fluid model in which the Knudsen resistance is ignored. The base case parameters are tortuosity = 1.5, catalyst surface area = 567 m^2/m^3 and catalyst thickness = 2 mm.

has the opposite effect. Decreasing the catalyst thickness reduces intra-catalyst resistances and so results in higher TAME production.

Our dusty fluid model also incorporates the Knudsen diffusivity, describing a diffusional resistance between the liquid and walls of the porous media, portrayed by the $Đ^e_{iM}$ coefficients. In our base case we had ignored the Knudsen resistance. Fig. 3(d) shows the bifurcation characteristics for this case, along with two other scenarios: (1) $Đ^e_{iM}$ is identical for all species and equal to the arithmetic average of the $Đ^e_{ij}$, (2) $Đ^e_{iM}$ is five times the value obtained in scenario (1). We note that for scenario (1) the TAME production is significantly lowered, whereas the simulation results following scenario (2) are almost identical to those for the base case (ignoring Knudsen contributions). We conclude that provided the Knudsen coefficients $Đ^e_{iM}$ are about 5 times higher than the $Đ^e_{ij}$, the Knudsen resistance can be ignored. The catalyst pore diameter is 160 nm; this value is large enough to justify the fact that the Knudsen diffusivities are large enough to be ignored; this conclusion follows from the procedures discussed in Wesselingh and Krishna [50] for estimation of $Đ^e_{iM}$.

The major conclusion to be drawn from the results shown in Fig. 3 is that the pseudo-homogenous model and the detailed heterogeneous model display essentially the same bifurcation features.

Fig. 4 shows the HSS and LSS predicted by the dusty fluid model when the reboiler load is 400 W. The TAME mole fraction profiles in the catalyst, liquid–solid film and liquid bulk phase computed at heights $z = 1.14$ m and $z = 1.39$ m are shown in Fig. 4(a) and (b). Fig. 4(c) and (d) show the TAME production rate and the recomputed catalyst effectiveness factor along the reactive section. The production rates predicted for the LSS and HSS are similar at the top half of the reactive section, whereas they differ quite significantly along the lower half of the catalytic section. Accordingly, the intra-catalyst TAME composition profiles near the top of the reactive section are similar for the LSS and HSS; Fig. 4(a). Since the TAME production rates near the top half of the reactive section are moderate in magnitude, utilisation of the catalyst is good and this is reflected in catalyst effectiveness factor approaches almost unity in this section (Fig. 4(c)). For the LSS the TAME production rates are moderate over the entire length of the reactive section and, consequently, the catalyst effectiveness is close to unity over the entire reactive section. In contrast, operating at the HSS, the TAME production rate shows a high peak in the lower half of the reactive section. This causes the catalyst effectiveness to decrease significantly below unity. However, it is interesting to note that the catalyst effectiveness in the lower half of the reactive section continues to decrease to low values even when the production rates decreases from the peak values to near-zero values (cf. Fig. 4(c) and (d)). This behaviour is closely related to the impact of the inverse reaction order of methanol concentration on the TAME production rates. Fig. 5(a) depicts the composition profiles along the catalytic section in a composition subspace of methanol and *n*-pentane (inert used in the reaction). For illustration of the impact of the inverse reaction order of methanol on the TAME production we present in Fig. 5(b) the production rate as a function of methanol and *n*-pentane mole fraction with the TAME mole fraction was fixed at 0.05. Note in both diagrams the methanol mole fractions are plotted on a logarithmic scale. When operating at a LSS the methanol mole fractions are evenly distributed in the reactive section and stay above around 0.2; see Fig. 5(a).

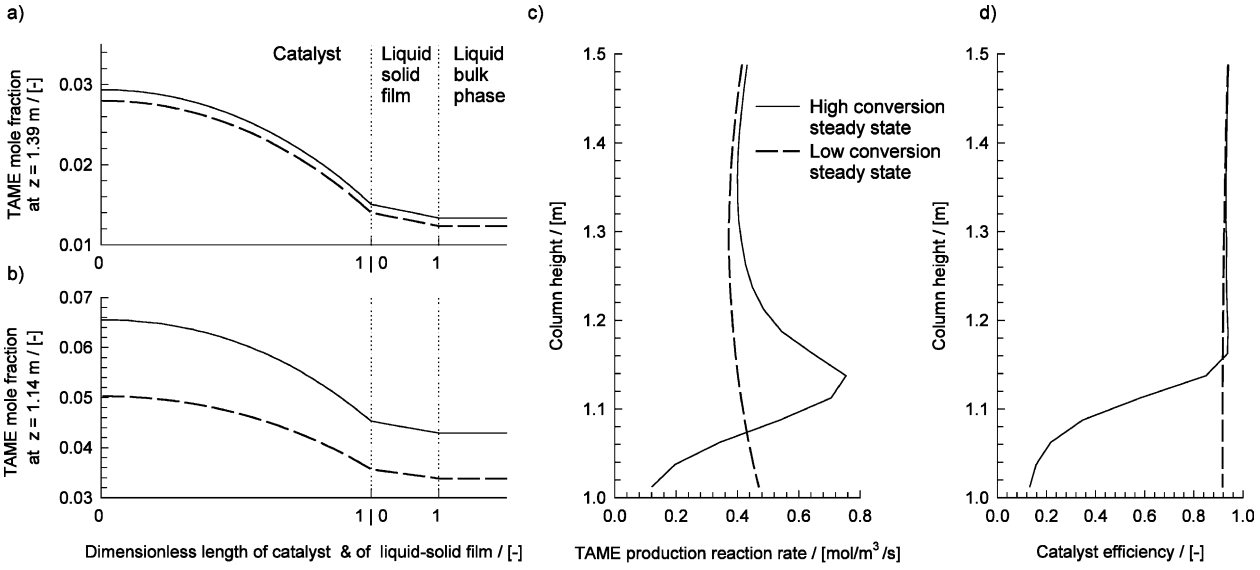

Fig. 4. HSS and LSSs predicted by the dusty fluid model. TAME concentration profiles at a column height of (a) 1.39 m and (b) 1.14 m. (c) TAME production rate per catalyst volume along the reactive section. (d) Catalyst efficiency along the reactive section. The reboiler load is 400 W.

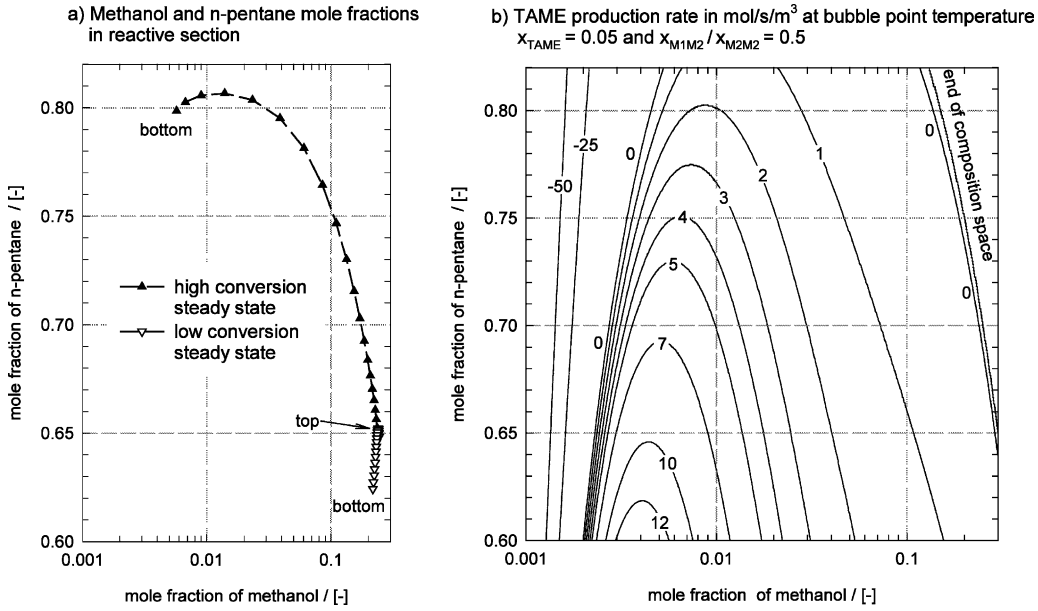

Fig. 5. (a) HSS and LSSs predicted by the dusty fluid model at a reboiler load of 400 W. Composition profile of the reactive section in the methanol–*n*-pentane composition subspace. (b) TAME production rate for varying methanol, *n*-pentane and isoamylene mole fractions. The mole fraction of TAME is kept constant at 0.05.

In contrast, the methanol composition profile for a HSS reaches values one magnitude lower at the bottom of the reactive section. As indicated in Fig. 5(b), the TAME production rate is very sensitive to any composition change in a region for small methanol concentration. Hence, intra-catalyst mass transfer resistances will affect production rates and also the catalyst effectiveness factors for low methanol concentrations.

We performed a series of simulations to study the bifurcation characteristics of the pseudo-homogenous model with varying catalyst effectiveness factors; these results are compared with the dusty fluid simulation results (for base case values of the parameters) in Fig. 6. The high conversion branch of a pseudo-homogenous model employing a catalyst effectiveness factor of 0.7 is close to corresponding branch of the dusty fluid model.

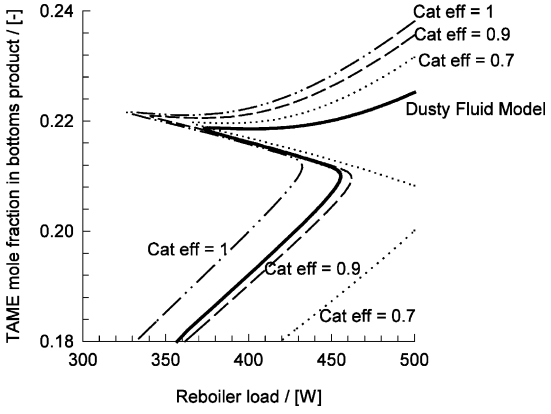

Fig. 6. Bifurcation diagrams of the dusty fluid model and the pseudo-homogenous model with catalyst efficiency factor ranging from 1.0 to 0.7.

On the other hand the low conversion branch of a pseudo-homogenous model employing a catalyst effectiveness factor of 0.9 approaches the low conversion branch of the dusty fluid model. We can conclude therefore that the bifurcation characteristics of the dusty fluid model can be captured in essence by a pseudo-homogenous description provided we use an appropriate catalyst effectiveness factor *for each branch in the bifurcation diagram*. We proceed to study the column dynamics of the TAME column with a pseudo-homogenous description.

4. Dynamics simulation of transition between steady states

Dynamic simulations require additional information about the liquid hold-up in the column, reboiler and condenser. The storage capacities of the condenser and reboiler have been estimated to be 1 l each. Since the pseudo-homogeneous model does not account for intra-particle mass storage in the catalyst we assumed a constant liquid hold-up in the catalyst with composition equal to the bulk phase. We estimated the time-independent (static) hold-up to be 0.23 l in the entire catalytic section and 0.33 l in the entire inert section. This estimate is based on taking 50% pore volume within the packing to consist of static liquid hold-up. The pore volume constitutes a fraction 0.39 of the packing volume for catalytic Raschig Rings and 0.55 for porous (inert) glass rings; see Mohl et al. [33]. The packing volume constitutes 53% of the column volume

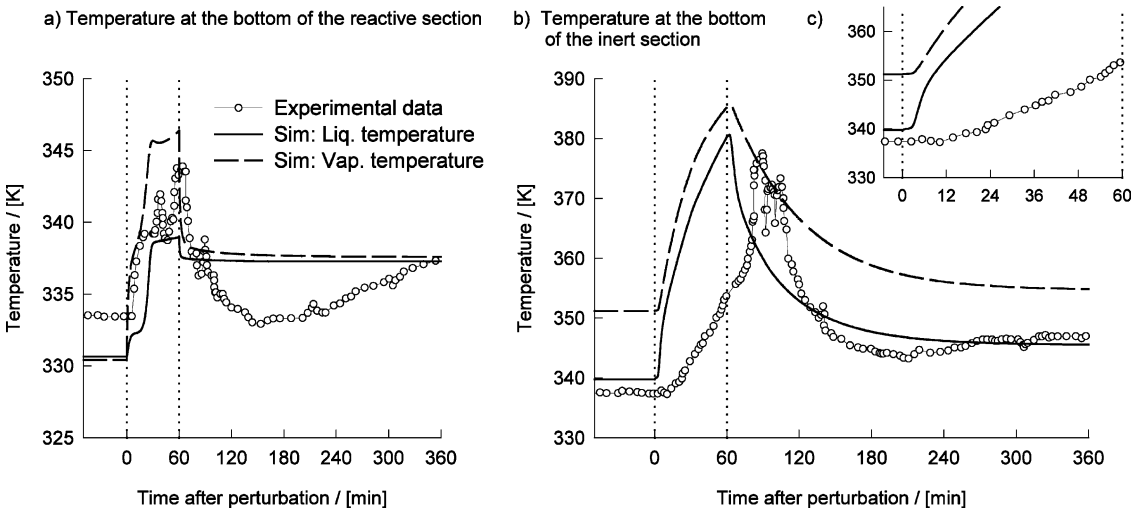

Fig. 7. Vapour and liquid temperature trajectories of low to high conversion steady state transition when switching the feed to pure TAME for 1 h. (a) Temperatures at the bottom of the catalytic section. (b) and (c) Temperatures at the bottom of the inert section.

(packing voidage = 47%). Superposed on these values of the static liquid hold-ups, is the dynamic liquid hold-up that depends on the flows of the vapour and liquid phases; this is estimated using the correlation of Mackowiak [51].

Consider steady-state operation at the low-conversion branch of the bifurcation diagram shown in Fig. 2(c) with the reboiler load fixed at 340 W. We adopted the perturbation scheme and the experimental data from Mohl et al. [33]; see Fig. 7. At the beginning of the perturbation ($t = 0$ min) the feed is switched to pure TAME while the flow rate is maintained. One hour later the feed was reset to its original values. Fig. 7 shows the predicted vapour and liquid temperatures. We see from Fig. 7 that the main dynamic features of the Mohl et al. experiments are captured by our model and the column undergoes a transition from a low to high conversion level. Fig. 7(a) shows the temperature at the bottom of the reactive section. The liquid and vapour temperature rises rapidly due to the vaporising pure TAME feed below the catalytic section. When the feed is reset at the end of the perturbation our model predicts a sharp drop in temperature and quickly recovers its final (high conversion) steady state. This trend does not correspond to the measurements of Mohl et al. [33], which show a large undershoot and it takes approximately another 4 h until the HSS is reached. Consider the bottom of the inert section. Our model matches the magnitude of the temperature peak quite well; see Fig. 7(b). However the model predicts a much sharper rise than observed experimentally. The main reason for the deviations between experiment and our dynamics simulations could be our imprecise knowledge of the two-phase hydrodynamics in the laboratory column.

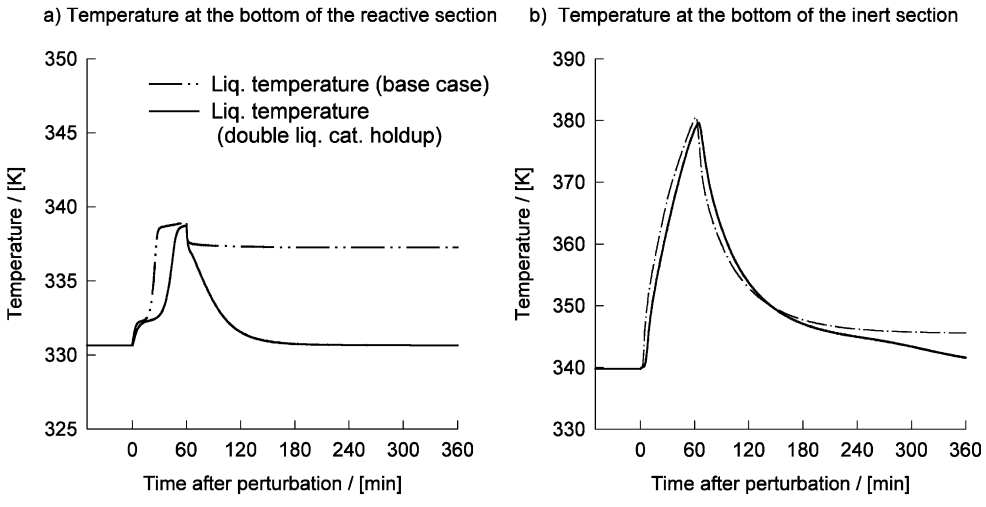

Fig. 8. Liquid temperature trajectories for the base case amount of static liquid hold-up in the catalyst and when it is doubled. The feed is switched to pure TAME for 1 h at $t = 0$ h.

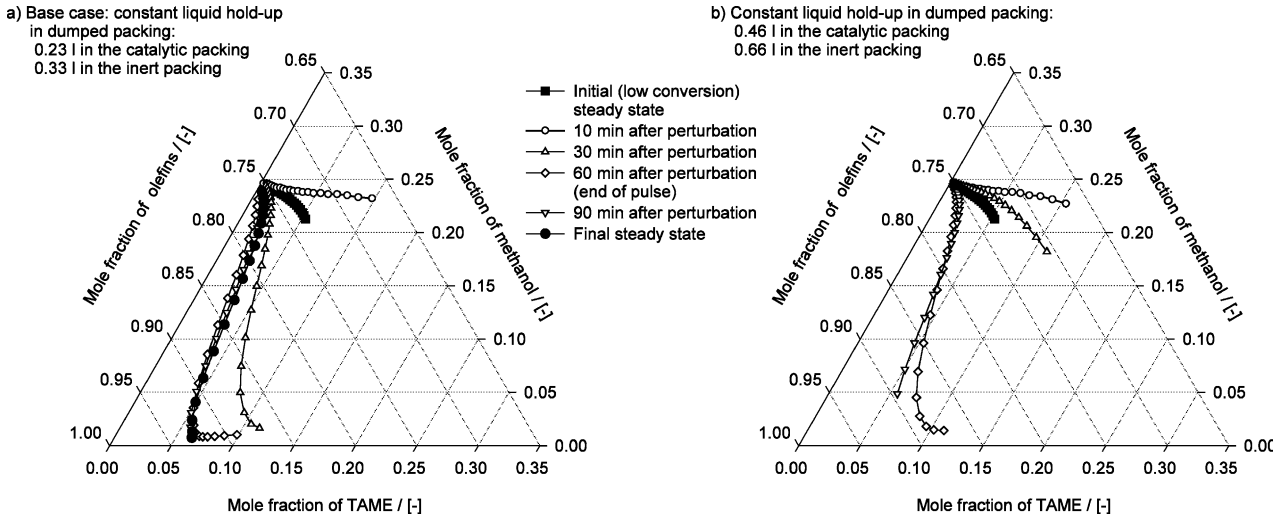

Fig. 9. Composition profiles for the base case amount of static liquid hold-up in the catalyst and when the static hold-up is doubled.

The static liquid hold-up is a particularly sensitive parameter and this sensitivity is illustrated in the simulation results in Fig. 8 that compares the base case dynamic simulations with that when the static liquid hold-up is doubled (0.46 l in the entire catalytic section and 0.66 l in the entire inert section). As expected the steady state behaviour is not influenced by variations in the static hold-up, but the dynamics is affected dramatically. In contrast to the base case no steady state transition is observed for increased static liquid hold-up; the original (low-conversion) steady state is recovered. We also note that the increase in temperature in the reactive section (Fig. 8(a)) is more gradual when the liquid hold-up is higher, but does not approach such a gentle climb as seen in the experiments. This indicates that the dynamic exchange of mass and heat between the catalyst and bulk phase seem to be essential with regard to recovery of experimental data. Fig. 8(a) also shows that the liquid temperature in the bottom of the catalytic section rises in two 'steps'. The first temperature rise is caused by an increase of TAME composition in the bottom of the reactive section after pure TAME is fed and vaporised. This happens almost simultaneously, both for low and high hold-up cases. The second temperatures ascent takes place about 20 min earlier for the base case.

The temperature rises are linked to changes in the composition profiles. Fig. 9 presents the composition profile along the reactive section in a ternary TAME–methanol–olefins composition space. The composition at the top of the reactive section is determined by the methanol-olefins azeotrope. Ten minutes after switching the feed to pure TAME, the composition profiles for both hold-up cases are still similar. At this moment the change of the composition profiles in the reactive section is mainly determined by the vaporised and partly reboiled TAME feed. Further accumulation of the heaviest component TAME in the (inert) stripping section cause an increase of the *n*-pentane mole fractions in the reactive section; see Fig. 9. As we have mentioned

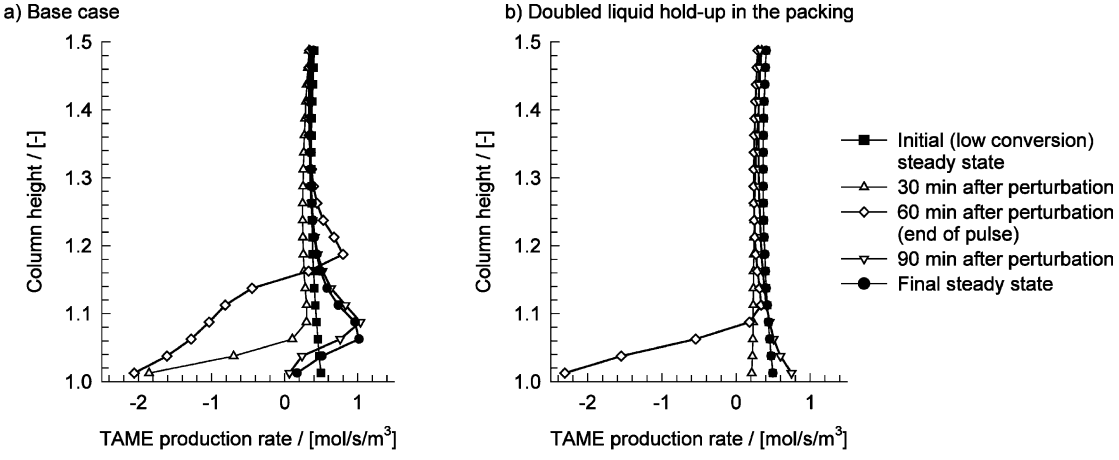

Fig. 10. TAME production rate profiles corresponding to the composition profiles shown in Fig. 9.

before the TAME production rate is sensitive in the range of small methanol mole fractions in the presence of sufficient iso-amylene and small TAME concentrations; see e.g. Fig. 5(b).

Corresponding simulation results for the production rates for the two hold-up cases are given in Fig. 10. Observing the production rates presented in Fig. 10 and the composition profiles of Fig. 9 exhibits low methanol concentrations for high *n*-pentane concentrations in the reactive section. When high TAME production rates are triggered and subsequently Methanol will be consumed, a steady state transition from the LSS to the HSS is possible. Fig. 9(a) and Fig. 10(a) present this scenario for the base case. Higher static liquid hold-up, however, dilutes the accumulation of TAME in the stripping section during the disturbance and so results in lower *n*-pentane concentrations in the reactive section. Higher residence times also will propagate the feed disturbance much more slowly. In this case high reaction rates will not be triggered and the system reverts back to its original LSS; see Fig. 9(b) and Fig. 10(b).

5. Conclusion

The RD column for TAME synthesis exhibits steady-state multiplicity. These features are captured by a pseudo-homogeneous description of the reaction kinetics. The use of a rigorous heterogeneous catalytic reaction model yields essentially the same bifurcation features. The essential features of the heterogeneous model can be captured by appropriate choice of the catalyst effectiveness factor. We find, however, that different values of the effectiveness factor have to be used for the high and low conversion branches of the bifurcation diagram.

Our dynamic NEQ model, using the pseudo-homogenous reaction description, is able to predict the steady-state transition in the experiments of Mohl et al. [33] starting at the low conversion branch of the bifurcation diagram. The precise transient behaviour is found to be very sensitive to the static liquid hold-up in the catalytic section. This underlines the need for a proper understanding of the hydrodynamics in order to describe the column dynamics.

Acknowledgements

RB and RK are grateful to The Netherlands Organization for Scientific Research (NOW-CW) for award of a ‘programmasubsidie’ to develop novel concepts in reactive separations technology.

References

[1] M.F. Doherty, M.F. Malone, Reactive distillation, Ind. Eng. Chem. Res. 36 (2000) 4325–4334.
[2] M.F. Doherty, M.F. Malone, Conceptual Design Of Distillation Systems, McGraw-Hill, New York, 2001.
[3] R. Taylor, R. Krishna, Modelling reactive distillation, Chem. Eng. Sci. 55 (2000) 5183–5229.
[4] C. Thiel, K. Sundmacher, U. Hoffmann, Residue curve maps for heterogeneously catalysed reactive distillation of fuel ethers MTBE and TAME, Chem. Eng. Sci. 52 (1997) 993–1005.
[5] R. Jacobs, R. Krishna, Multiple solutions in reactive distillation for methyl *tert* butyl ether synthesis, Ind. Eng. Chem. Res. 32 (1993) 1706–1709.
[6] S.A. Nijhuis, F.P.M. Kerkhof, A.N.S. Mak, Multiple steady states during reactive distillation of methyl *tert*-butyl ether, Ind. Eng. Chem. Res. 32 (1993) 2767–2774.
[7] S. Hauan, T. Hertzberg, K.M. Lien, Multiplicity in reactive distillation of MTBE, Comput. Chem. Eng. 21 (1997) 1117–1124.
[8] T.E. Güttinger, M. Morari, Predicting multiple steady states in equilibrium reactive distillation. 1. Analysis of nonhybrid systems, Ind. Eng. Chem. Res. 38 (1999) 1633–1648.
[9] T.E. Güttinger, M. Morari, Predicting multiple steady states in equilibrium reactive distillation. 2. Analysis of hybrid systems, Ind. Eng. Chem. Res. 38 (1999) 1649–1665.
[10] E.Y. Kenig, A. Gorak, Modeling of reactive absorption using the Maxwell–Stefan equations, Ind. Eng. Chem. Res. 36 (1997) 4325–4334.
[11] E. Kenig, K. Jakobsson, P. Banik, J. Aittamaa, A. Gorak, M. Koskinen, P. Wettman, An integrated tool for synthesis and design of reactive distillation, Chem. Eng. Sci. 54 (1999) 1347–1352.
[12] L.U. Kreul, A. Gorak, C. Dittrich, P.I. Barton, Dynamic catalytic distillation: advanced simulation and experimental validation, Comput. Chem. Eng. 22 (1998) S371–S378.
[13] R. Baur, A.P. Higler, R. Taylor, R. Krishna, Comparison of equilibrium stage and non-equilibrium stage models for reactive distillation, Chem. Eng. J. 76 (2000) 33–47.
[14] A. Higler, R. Taylor, R. Krishna, Modeling of a reactive separation process using a nonequilibrium stage model, Comput. Chem. Eng. 22 (1998) S111–S118.
[15] A.P. Higler, R. Taylor, R. Krishna, Nonequilibrium modelling of reactive distillation: multiple steady states in MTBE synthesis, Chem. Eng. Sci. 54 (1999) 1389–1395.
[16] A.P. Higler, R. Taylor, R. Krishna, The influence of mass transfer and liquid mixing on the performance of reactive distillation tray column, Chem. Eng. Sci. 54 (1999) 2873–2881.
[17] A. Higler, R. Krishna, R. Taylor, A non-equilibrium cell model for packed distillation columns. The influence of maldistribution, Ind. Eng. Chem. Res. 38 (1999) 3988–3999.
[18] A. Higler, R. Krishna, R. Taylor, Non-equilibrium cell model for multicomponent (reactive) separation processes, AIChE J. 45 (1999) 2357–2370.
[19] A. Higler, R. Krishna, R. Taylor, Non-equilibrium modelling of reactive distillation: A dusty fluid model for heterogeneously catalysed processes, Ind. Eng. Chem. Res. 39 (2000) 1596–1607.
[20] R. Baur, R. Taylor, R. Krishna, J.A. Copati, Influence of mass transfer in distillation of mixtures with a distillation boundary, Chem. Eng. Res. Des., Trans. I. Chem. E. 77 (1999) 561–565.
[21] R. Baur, R. Taylor, R. Krishna, Development of a dynamic nonequilibrium cell model for reactive distillation tray columns, Chem. Eng. Sci. 55 (2000) 6139–6154.
[22] R. Baur, R. Taylor, R. Krishna, Dynamic behaviour of reactive distillation tray columns described with a nonequilibrium cell model, Chem. Eng. Sci. 56 (2001) 1721–1729.

[23] R. Baur, R. Taylor, R. Krishna, Dynamic behaviour of reactive distillation columns described by a nonequilibrium stage model, Chem. Eng. Sci. 56 (2001) 2085–2102.
[24] R. Baur, R. Taylor, R. Krishna, Influence of column hardware on the performance of reactive distillation columns, Catal. Today 66 (2001) 225–232.
[25] A. Kumar, P. Daoutidis, Modeling, analysis and control of ethylene glycol reactive distillation column, AIChE J. 45 (1999) 51–68.
[26] V.H. Agreda, L.R. Partin, W.H. Heise, High-purity methyl acetate via reactive distillation, Chem. Eng. Prog. 2 (1990) 40–46.
[27] L.U. Kreul, A. Gorak, P.I. Barton, Modeling of homogeneous reactive separation processes in packed columns, Chem. Eng. Sci. 54 (1999) 19–34.
[28] Sundamacher, K (1995) Reaktivdestillation mit katalytischen fuellkoerperpackungen—ein neuer Process zur Herstellung der Kraftstoffkomponente MTBE, Ph.D thesis, Universität Clausthal.
[29] K. Sundmacher, U. Hoffmann, Multicomponent mass transfer and energy transport on different length scales in a packed reactive distillation column for heterogeneously catalysed fuel ether production, Chem. Eng. Sci. 49 (1994) 4443–4464.
[30] K. Sundmacher, U. Hoffmann, Development of a new catalytic distillation process for fuel ethers via a detailed nonequilibrium model, Chem. Eng. Sci. 51 (1996) 2359–2368.
[31] K. Sundmacher, G. Uhde, U. Hoffmann, Multiple reactions in catalytic distillation processes for the production of the fuel oxygenates MTBE and TAME: analysis by rigorous model and experimental validation, Chem. Eng. Sci. 54 (1999) 2839–2847.
[32] P. Rapmund, K. Sundmacher, U. Hoffmann, Multiple steady states in a reactive distillation column for the production of the fuel ether TAME part II: experimental validation, Chem. Eng. Technol. 21 (1998) 136–139.
[33] K.D. Mohl, A. Kienle, E.D. Gilles, P. Rapmund, K. Sundmacher, U. Hoffmann, Steady state multiplicities in reactive distillation columns for the production of fuel ethers MTBE and TAME: theoretical analysis and experimental verification, Chem. Eng. Sci. 54 (1999) 1029–1043.
[34] R. Krishna, J.A. Wesselingh, The Maxwell–Stefan approach to mass transfer, Chem. Eng. Sci. 52 (1997) 861–911.
[35] R.C. Reid, J.M. Prausnitz, B.M. Poling, The Properties of Gases And Liquids, fourth ed., McGraw-Hill, New York, 1988.
[36] R.P. Danner, T.E. Daubert, Manual For Predicting Chemical Process Design Data, American Institute of Chemical Engineers, New York, 1983.
[37] R. Taylor, R. Krishna, Multicomponent Mass Transfer, Wiley, New York, 1993.
[38] H.A. Kooijman, R. Taylor, The ChemSep book, Libri Books (2001). Available from www.chemsep.org.
[39] H.A. Kooijman, Dynamic Nonequilibrium Column Simulation Ph.D. Dissertation, Clarkson University, Potsdam, USA, 1995.
[40] M. Michelsen, An efficient general purpose method of integration of stiff ordinary differential equations, AIChE J. 22 (1976) 594–597.
[41] R. Bulirsch, J. Stoer, Numerical treatment of ordinary differential equations by extrapolation methods, Numerical Math. 8 (1966) 1–13.
[42] R. Taylor, H.A. Kooijman, J.S. Hung, A second generation nonequilibrium model for computer simulation of multicomponent separation processes, Comput. Chem. Eng. 18 (1994) 205–217.
[43] T.L. Wayburn, J.D. Seader, Homotopy continuation methods for computer aided process design, Comput. Chem. Eng. 11 (1987) 7–25.
[44] M. Kubicek, Algorithm 502, dependence of a solution of nonlinear systems on a parameter, ACM. Trans. Math. Softw. 2 (1976) 98–107.
[45] C. Oost, K. Sundmacher, U. Hoffmann, The synthesis of tertiary amyl methyl ether (TAME): equilibrium of the multiple reactions, Chem. Eng. Technol. 18 (1995) 110–117.
[46] C. Oost, U. Hoffmann, The synthesis of tertiary amyl methyl ether (TAME): microkinetics of the reactions, Chem. Eng. Sci. 51 (1996) 329–340.
[47] L.K. Rihko, A.O.I. Krause, Kinetics of heterogeneously catalyzed tert-amyl methyl ether reactions in the liquid phase, Ind. Eng. Chem. Res. 34 (1995) 1172–1180.
[48] L.K. Rihko, P. Kiviranta Paakkonen, A.O.I. Krause, Kinetic model for the etherification of isoamylenes with methanol, Ind. Eng. Chem. Res. 36 (1997) 614–621.
[49] P. Kiviranta-Paakkonen, L. Struckmann, A.O.I. Krause, Comparison of the various kinetic models of TAME formation by simulation and parameter estimation, Chem. Eng. Technol. 21 (1998) 321–326.
[50] J.A. Wesselingh, R. Krishna, Mass Transfer in Multicomponent Mixtures, Delft University Press, Delft, 2000.
[51] J. Mackowiak, Fluiddynamik von Kolonnen mit modernen Füllkörpern und Packungen für Gas/Flüssigkeitssysteme, Sauerländer, Aarau, 1991.